STUDY ON THE MECHANISM OF TURBULENT ENTRAINMENT THROUGH 3D-PTV AND DNS

Markus Holzner, Beat Lüthi, Wolfgang Kinzelbach
Institut für Umweltingenieurwissenschaften,
ETH Zürich
Wolfgang-Pauli-Str. 15, CH-8093 Zürich
holzner,luethi,kinzelbach@ifu.baug.ethz.ch

Alexander Liberzon
Dept. Fluid Mechanics and Heat Transfer,
Tel Aviv University
Ramat Aviv 69978, Israel
alexlib@eng.tau.ac.il

Nikolay Nikitin
Institute of Mechanics,
Moscow State University
119899 Moscow, Russia
NVNikitin@mail.ru

Michele Guala
Swiss Federal Institute for Snow and Avalanche Research,
Flüelastrasse 11, CH-7260 Davos
Guala@slf.ch

Arkady Tsinober
Institute for Mathematical Sciences and Department of Aeronautics,
Imperial College London
53 Princes Gate, Exhibition Road, South Kensington Campus, London, UK
a.tsinober@imperial.ac.uk

ABSTRACT

The work reported below is an analysis of small scale properties of turbulent flow without strong mean shear in a homogeneous Newtonian fluid in proximity of the turbulent/non-turbulent interface. The main tools used are a three-dimensional particle tracking system (3D-PTV) allowing to measure and follow in a Lagrangian manner the field of velocity derivatives and direct numerical simulations (DNS). The study is based on the statistical analysis of flow tracers crossing the turbulent/non-turbulent interface. The analysis of flow properties in the proximity of the interface allows for direct observation of the key physical processes underlying the entrainment phenomenon. We found that both, viscous and inertial processes are important for the increase of enstrophy at the turbulent/non-turbulent interface.

INTRODUCTION

Turbulent entrainment is the process of transition of fluid from laminar to turbulent state through the boundary between the two (Tsinober, 2001) and it occurs in so-called 'partly turbulent' flows, such as free shear flows (jets, plumes, wakes, mixing layers), penetrative convection in the atmosphere and in the ocean, gravity currents and avalanches. One essential and physically qualitative distinction between turbulent and non-turbulent regions is that turbulent regions are rotational, whereas the non-turbulent ones are (practically) irrotational (Corrsin and Kistler, 1954, 1955). In particular, the two regions are separated by a sharp interface, called 'viscous sublayer' by Corrsin and Kistler (1954, 1955), as viscous diffusion of vorticity is believed to be dominant across this interface. However, at large Reynolds numbers, the entrainment rate and the propagation velocity of the interface relative to the fluid are known to be independent of viscosity (e.g., Townsend, 1976, Tsinober, 2001, and references therein). Therefore, the slow process of diffusion into the ambient fluid must be accelerated by interaction of velocity fields of eddies of all sizes, from viscous eddies to the energy-containing eddies so that the overall rate of entrainment is set by large-scale parameters of the flow (Tsinober, 2001). However, it is not known exactly how the slow process of diffusion into the ambient fluid is accelerated by interaction of eddies of all sizes. Until recently it was difficult to address these questions, as it requires information on small scale vorticity and strain, which experimentally was not accessible. This is why very little is known about the processes at small scales and in the proximity of the interface. While in previous studies the en-

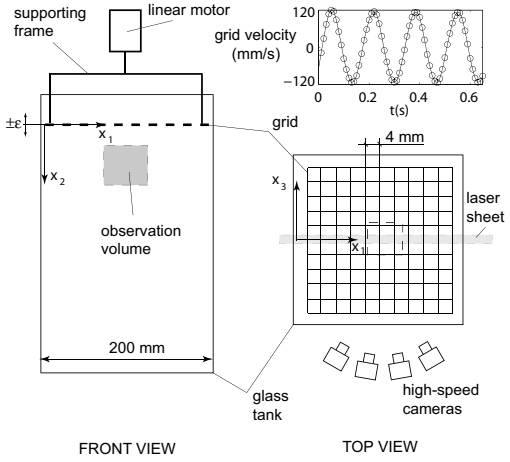

Figure 1: Schematic of the experimental setup. A time sample of the grid velocity obtained from the encoder signal is shown in the upper right corner.

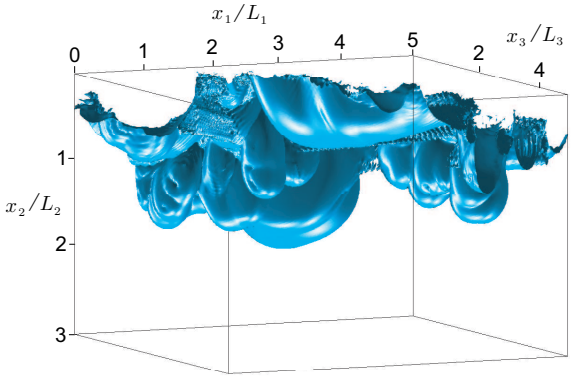

Figure 2: Vorticity iso-surface snapshot obtained from DNS.

trainment process was mostly examined in free shear flows (e.g., Bisset et al., 2002, Corrsin and Kistler, 1954, 1955, Mathew and Basu, 2002, Townsend, 1976, Westerweel et al., 2005) and boundary layers (e.g., Corrsin and Kistler, 1954, 1955), the focus here is on some simple, but basic aspects. A turbulent front is induced by the action of planar forcing, such that the resulting turbulent flow is quasi-homogeneous in plane and the turbulent interface spreads on average along one dimension. The present study is part of an ongoing research project with previous results published in Holzner et al. (2006, 2007). We report a comparison between three-dimensional flow measurements obtained through scanning particle tracking velocimetry (SPTV) and direct numerical simulation (DNS).

METHOD

Experimentally, a turbulent/non-turbulent interface was realized by using the oscillating planar grid described in Holzner et al. (2006). A schematic of the experimental setup is shown in Figure 1. The grid is a fine woven screen installed near the upper edge of a water filled glass tank and it oscillates at a frequency of 6 Hz and an amplitude of 4 mm. The scanning method of 3D particle tracking velocimetry used for the measurements is described in detail in Hoyer et al. (2005). 3D-SPTV is a flexible flow measurement technique based on the processing of stereoscopic images of flow tracer particles. As in Holzner et al. (2007), the derivatives of velocity, $\partial u_i/\partial x_j$, and Lagrangian acceleration, $\partial a_i/\partial x_j$, were calulated along particle trajectories and subsequently interpolated on an Eulerian grid. The Laplacian of vorticity, $\nabla^2\boldsymbol{\omega}$, is obtained from the local balance equation of vorticity in the form $\nabla\times\mathbf{a}=\nu\nabla^2\boldsymbol{\omega}$ by evaluating the term $\nabla\times\mathbf{a}$ from the Lagrangian tracking data. The experimental error associated with measurements of derivatives of acceleration is significant. Erroneous values of $\nu\nabla^2\boldsymbol{\omega}$ are filtered using the following criterion based on the enstrophy balance equation:

$$\delta_v = \frac{|\frac{D}{Dt}\frac{\omega^2}{2} - \omega_i\omega_j s_{ij} - \nu\omega_i\nabla^2\omega_i|}{|\frac{D}{Dt}\frac{\omega^2}{2}| + |\omega_i\omega_j s_{ij}| + |\nu\omega_i\nabla^2\omega_i|} \leq 0.2. \qquad (1)$$

The available data is decreased substantially by the filtering as only 20% survives. This is one of the reasons why the results are compared to DNS. The number of tracked particles per frame is about $6{\cdot}10^3$ in a volume of $2{\times}2{\times}1.5$ cm^3 about 2 cm away from the grid and the mean interparticle distance is about 1 mm, which is slightly above the estimated Kolmogorov length scale, η=0.6 mm. We estimated η using $\eta=(\nu^3/\epsilon)^{1/4}$, where ν is the kinematic viscosity of the fluid, $\epsilon=2\nu\langle s^2\rangle$ is the measured dissipation ($s^2=s_{ij}s_{ij}$ is the rate of strain and s_{ij} are the components of the rate of strain tensor). The Taylor microscale, λ, is about 7 mm. The spacing of the Eulerian grid was taken equal to the interparticle distance. The estimated Kolmogorov time scale is τ_η=0.3 s, which is about 7 times the time-interval between two volume-scans, Δt=0.02 s. In both experiment and simulation, the Taylor microscale Reynolds number is Re_λ=50.

Direct numerical simulation (DNS) was performed in a box (side-length $5L_1$, $5L_2$, $3L_3$) of initially still fluid. Random (in space and time) velocity perturbations are applied at the boundary x_2=0. The procedure of generating the boundary conditions is as follows. For a fixed time and in the discrete set of points, $x_1=k\Delta_l$, $x_3=l\Delta_l$ (k, l - integers), each velocity component, u_i (i = 1, 2, 3), is calculated as $u_i=V_i\xi$, where ξ is a random number within the interval $[-1,1]$ and V_i is a given velocity amplitude. For other times and spatial points (x_1, x_3) boundary velocities are obtained by cubic interpolation in time and bilinear interpolation in space. At each time the three boundary velocity components yield zero average value over the boundary plane. The method of boundary velocity assignment determines the velocity scale, $V=\max(V_i)$ and the length scale Δ_l. The corresponding time scale is defined as $\Delta_t=\Delta_l/V$. Together with the viscosity of a fluid, ν, these parameters define the Reynolds number $Re=V\Delta_l/\nu=1000$ of the simulation. The Navier-Stokes equations are solved with periodic boundary conditions for the directions x_1 and x_3, with periods L_1 and L_3, respectively. The computational domain is finite in the x_2 direction, as $x_2\leq 3L_2$. Shear-free conditions $\partial u_1/\partial x_2=\partial u_3/\partial x_2=u_2=0$ are imposed at the boundary $x_2=L_2$. A mixed spectral-finite-difference method is used for the spatial discretization and the time advancement is computed by a semi-implicit Runge-Kutta method (Nikitin, 1994, 1996). The resolution is 192×192 Fourier modes in x_1 and x_3 directions and 192 grid points in x_2 direction. The analysis is done for times when the turbulent/non-turbulent interface is about half a box size away from the source. The local Kolmogorov length scale is twice the grid spacing. The

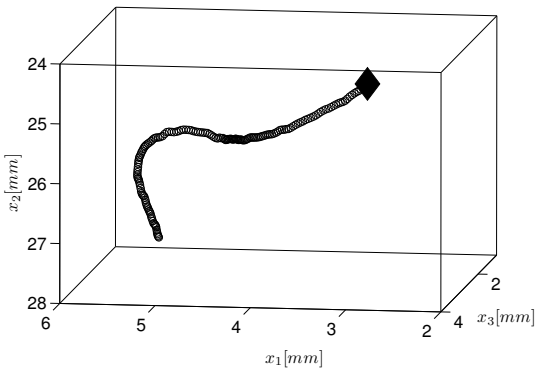

Figure 3: Single trajectory plotted in real space. The symbol '♦' indicates the initial position.

paths of 4000 fluid particles have been calculated using

$$\frac{D\mathbf{x}}{Dt} = \mathbf{u}(\mathbf{x}, t), \tag{2}$$

where $\mathbf{x}$ is the position of the fluid particle at time t. For the time integration of the particle position a 3rd order explicit Runge-Kutta scheme was used. The velocity and other quantities of interest were interpolated to the trajectory point using a bilinear interpolation in space. The fluid particles were released at t/Δ_t=5 and integrated until t/Δ_t=10. Their initial positions are regularly distributed in a subregion of the computational domain ($2.5 < x_1/L_1 < 3.5$, $1.2 < x_2/L_2 < 2.2$ and $2.5 < x_3/L_3 < 3.5$), in proximity of the vorticity surface shown in Figure 2. The characteristic properties of the experiment and the simulation are summarized in Table 1.

	Δx_k	Δt	Re_λ
3D-SPTV	1 mm	0.02 s	50
DNS	$8 \cdot 10^{-3}\Delta_l$	$2 \cdot 10^{-3}\Delta_l/V$	50
	$\tau_\eta/\Delta t$	$\eta/\Delta x_k$	$\lambda/\Delta x_k$
3D-SPTV	15	0.6	7
DNS	300	2.0	28

Table 1: Characteristic properties of the flow for the experiment and the simulation.

RESULTS

In both experiment and simulation, turbulence is generated at the plane x_2=0 and propagates mainly along $x_2 >$0. In the previous study of Holzner et al. (2007) the main focus was on the relation of small scale quantities with the distance to the interface. The present investigation concentrates on the evolution of some of these properties in a Lagrangian frame of reference, that is, fluid tracers crossing the turbulent/non-turbulent interface are analyzed. For each particle trajectory, the point in time, t^*, when the interface is crossed was identified using a fixed threshold of enstrophy, $\omega^2 = \omega_i\omega_i$, for details see Holzner et al. (2006, 2007) and references therein. Particular attention is on terms in the balance equation of enstrophy, which reads

$$\frac{D}{Dt}\frac{\omega^2}{2} = \omega_i\omega_j s_{ij} + \nu\omega_i\nabla^2\omega_i \tag{3}$$

and on some terms in the analogous equation for the rate of strain, written as

$$\frac{D}{Dt}\frac{s^2}{2} = -s_{ij}s_{jk}s_{ki} - \frac{1}{4}\omega_i\omega_j s_{ij} - s_{ij}\frac{\partial^2 p}{\partial x_i \partial x_j} + \nu s_{ij}\nabla^2 s_{ij}. \tag{4}$$

Figure 3 shows a representative particle trajectory in real space with initial position in the non-turbulent region measured through 3D-SPTV. To obtain a first impression of the entrainment process in a Lagrangian frame, time series of several quantities along this trajectory are plotted in Figure 4. The time axis is centered at the point t^*, i.e. $\hat{t} = t - t^*$, and normalized by τ_η. Figure 4a shows the evolution of ω^2, $2s^2$ and the second invariant of the velocity gradient tensor, $Q = 1/4(\omega^2 - 2s^2)$. We observe that ω^2 is initially very low and increases attaining values close to the intensity of strain. In contrast to enstrophy, strain is already significantly high in the non-turbulent region and increases more gradually. This difference in magnitudes between ω^2 and $2s^2$ is an important feature of the process, since in fully developed turbulence enstrophy and strain are 'equal partners' (e.g., Tsinober, 2001). Notably, the invariant Q reaches a local minimum in correspondence of $\hat{t}$=0. Figure 4b illustrates the evolution production terms of enstrophy and strain together with the third invariant of the velocity gradient tensor, $R = -1/3(s_{ij}s_{jk}s_{ki} + 3/4\omega_i\omega_j s_{ij})$. Similar to ω^2 and s^2, $\omega_i\omega_j s_{ij}$ is low in the non-turbulent region, while $-s_{ij}s_{jk}s_{ki}$ is not small. With time, they both grow in magnitude and become of comparable intensity. Similar to Q before, the third invariant R shows a local maximum close to the origin. Since the mean values of Q and R vanish identically for homogeneous turbulence, their nonzero values indicate that the particle path traverses regions with some degree of inhomogeneity. Next, the evolution of the terms of Eq. 3 are shown in Figure 4c. It turns out that both, $\omega_i\omega_j s_{ij}$ and $\nu\omega_i\nabla^2\omega_i$ are positive and contribute to the growth of $\frac{D}{Dt}\frac{\omega^2}{2}$. Compared to $\nu\omega_i\nabla^2\omega_i$, the production term, $\omega_i\omega_j s_{ij}$, is initially smaller in magnitude, but grows quickly and becomes the major responsible term for the growth of $\frac{D}{Dt}\frac{\omega^2}{2}$, while the viscous term reaches a local maximum before it becomes negative. For the statistical analysis, the measured and simulated particle trajectories are averaged defining an ensemble of events, similar to the procedure described in Holzner et al. (2006, 2007). All trajectories with initial position in the non-turbulent region are centered at the point t^* introduced above and subsequently they are ensemble averaged. For the experiment, about $3{\cdot}10^3$ with an average length of $4\tau_\eta$ were processed in this way. The number of points considered for the statistics is $2{\cdot}10^5$. In the simulation, out of the $4{\cdot}10^3$ trajectories about 300 could be processed with a total number of $5{\cdot}10^5$ data points. The value of the threshold was set to 5% of the mean value of ω^2 in the turbulent region. This parameter was varied between 1-25% (numerically, this is equivalent to 0.1-2.5 s^2) and it was verified that, at least on the qualitative level, all the results remained valid.

As discussed above for the individual trajectory (more examples are shown in Figure 5), we note that the viscous term $\nu\omega_i\nabla^2\omega_i$ exhibits a remarkable behavior showing a distinct maximum during the crossing of the interface. Therefore, we use the maximum of the viscous term as the exact location of the interface, defined in a physically more appealing way than the threshold-dependent time moment t^*. For the further analysis we define three physically distinct regions of the interface with respect to the maximum of $\nu\omega_i\nabla^2\omega_i$ (marked in Figure 5): (A) the *turbulent* region, in which the behavior of the viscous term is 'normal', i.e. it

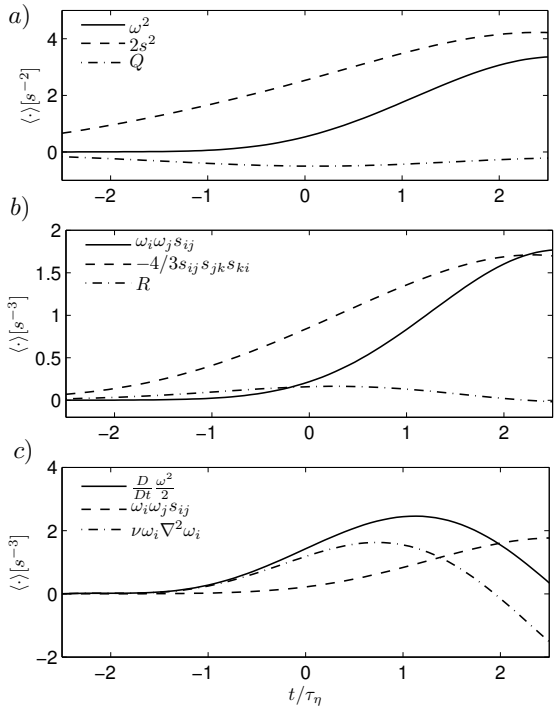

Figure 4: Lagrangian evolution of quantities along the trajectory plotted in Figure 3. The time axis is normalized by the Kolmogorov time scale, τ_η.

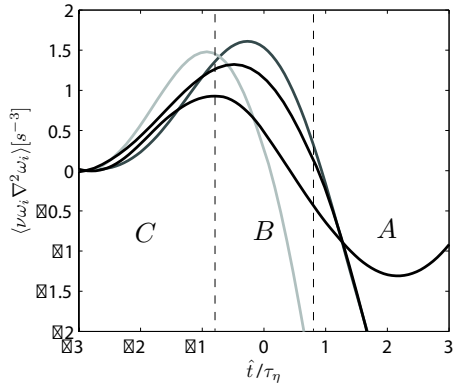

Figure 5: Individual Lagrangian trajectories of $\nu\omega_i\nabla^2\omega_i$ obtained from PTV.

is mainly negative like in fully developed stationary turbulence, where the term is negative in the mean (e.g., Tsinober, 2001), (B) the interval between the peak and the point where $\nu\omega_i\nabla^2\omega_i$=0 is termed *intermediate* region (with the 'abnormal' viscous production) and, (C) the *non-turbulent* region from the peak to $\hat{t}/\tau_\eta$=-3. It is instructive to look at the properties of the inertial and viscous terms of Eq. 3 in the three regions, separately. We represent enstrophy production as a scalar product of the vorticity vector and the vortex stretching vector, $W_i = \omega_j s_{ij}$, as $\omega_i\omega_j s_{ij} = \boldsymbol{\omega}\cdot\mathbf{W}$. In analogy we can write the viscous term as $\nu\omega_i\nabla^2\omega_i = \nu\boldsymbol{\omega}\cdot\nabla^2\boldsymbol{\omega}$.

For a closer inspection of the nature of enstrophy production in the region of the interface we show PDF's of the cosine between vorticity, $\boldsymbol{\omega}$, and the vortex stretching vector,

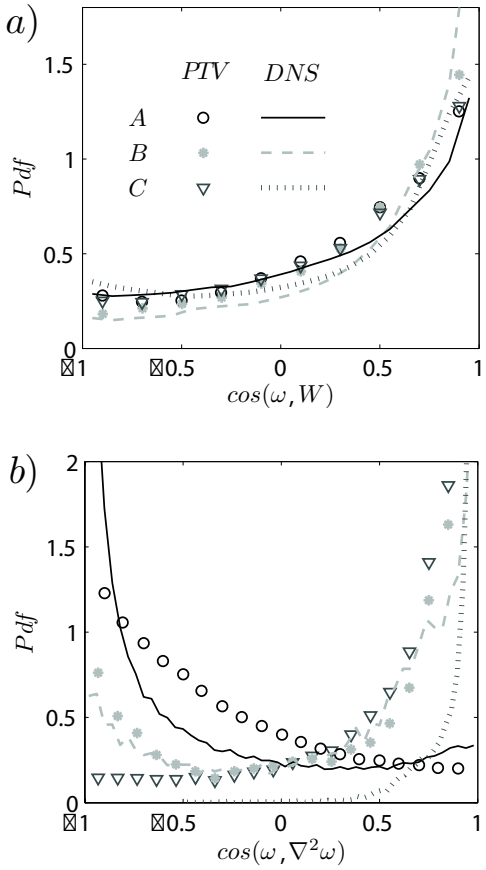

Figure 6: PDF's of the cosine between vorticity, $\boldsymbol{\omega}$, and the vortex stretching vector, $\mathbf{W}$ (a) and the cosine between vorticity, $\boldsymbol{\omega}$, and the Laplacian of vorticity, $\nabla^2\boldsymbol{\omega}$ (b), for the three regions.

$\mathbf{W}$, as obtained from PTV and DNS in Figure 6a. The physical interpretation of the geometrical invariant cos($\boldsymbol{\omega}$,$\mathbf{W}$) is straight-forward. It is positive when the projection of the vortex stretching vector, $\mathbf{W}$, on $\boldsymbol{\omega}$ points in the same direction as vorticity and thus, vortex stretching actually occurs. If cos($\boldsymbol{\omega}$,$\mathbf{W}$) is zero it will only attempt to tilt the direction of $\boldsymbol{\omega}$ and if it is negative then vorticity is compressed. We see that in region A the PDF is clearly positively skewed. The positive skewness of this PDF is a well known genuine property of turbulence and one of the main reasons for the positiveness of the mean enstrophy production, $\langle\omega_i\omega_j s_{ij}\rangle$ >0 (see Tsinober, 2001, Lüthi et al., 2005, and references therein). Interestingly, the positive skewness is slightly increased in region B, while in region C it is again comparable to region A. Figure 6b shows the cosine of the angle between vorticity and its Laplacian, $\nabla^2\boldsymbol{\omega}$, which exhibits significant changes across the regions A,B and C. The observed transition from positive (alignment, region C) to negative (anti-alignment, region A) values is in agreement with the qualitatively different behavior of $\nu\omega_i\nabla^2\omega_i$ in these regions observed from the individual trajectories shown before. The results indicate that an interpretation of the viscous term $\nu\omega_i\nabla^2\omega_i$ as *interaction between strain and vorticity due to viscosity* (i.e. due to the curl of the viscous force originating from the divergence of the strain tensor) is physically more appealing than 'simple' diffusion of vorticity due to viscosity. We emphasize that $\nu\omega_i\nabla^2\omega_i$ is

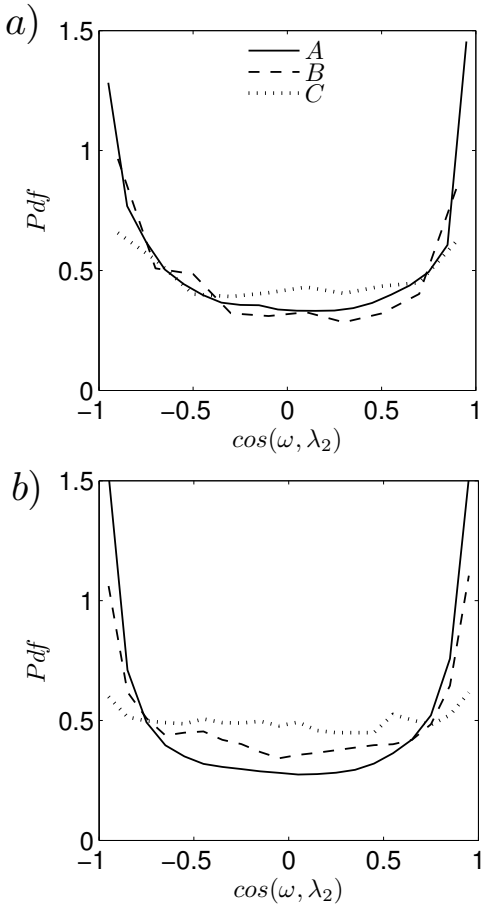

Figure 7: PDF's of the cosine between vorticity, $\boldsymbol{\omega}$, and the intermediate eigenvector of the rate of strain tensor, $\boldsymbol{\lambda_2}$, for the three regions from PTV (a) and DNS (b).

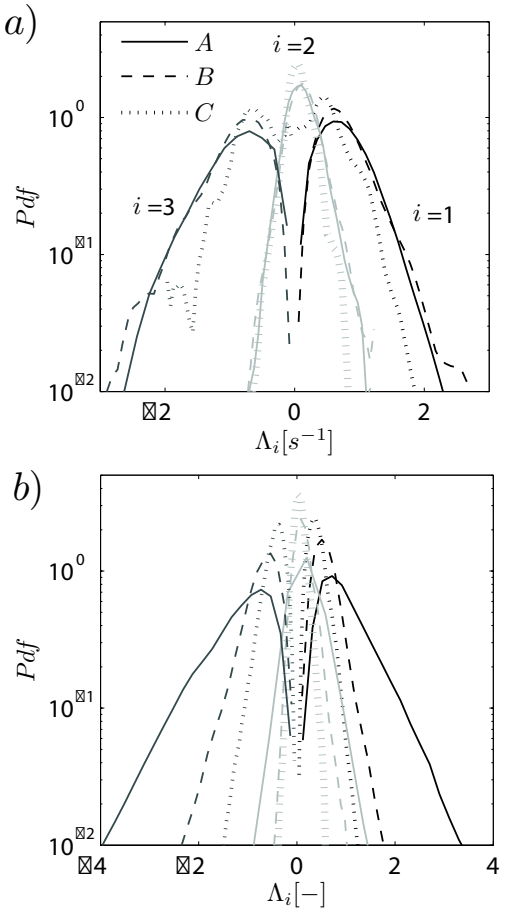

Figure 8: PDF's of the eigenvalues of the rate of strain tensor, Λ_i, for the three regions from PTV (a) and DNS (b).

the interaction of vorticity and strain since (e.g., Batchelor, 2000) $\nu\nabla^2\boldsymbol{\omega}= 1/\rho\ \nabla\times\mathbf{F}^s$, where $F_i^s = 2\nu\partial/\partial x_k\{s_{ik}\}$ and ρ is the fluid density.

It is also instructive to invoke another useful geometrical interpretation related to the enstrophy production term, namely, we write

$$\omega_i\omega_j s_{ij} = \omega^2\Lambda_i cos^2(\boldsymbol{\omega},\boldsymbol{\lambda_i}), \tag{5}$$

where $\boldsymbol{\lambda_i}$ denotes the eigenvectors of the rate of strain tensor and Λ_i its eigenvalues. From Eq. 5 we see that the effectiveness of $\omega_i\omega_j s_{ij}$ is related to the orientation of $\boldsymbol{\omega}$ relative to the eigenframe of the rate of strain tensor, $cos(\boldsymbol{\omega},\boldsymbol{\lambda_i})$. The preferential alignment of $\boldsymbol{\omega}$ with the intermediate eigenvector, $\boldsymbol{\lambda_2}$, is a well known characteristic property of turbulence (Siggia, 1981, Ashurst et al., 1987, Tsinober, 2001, Lüthi et al., 2005). The PDF's of the cosine between $\boldsymbol{\omega}$ and $\boldsymbol{\lambda_2}$ are plotted in Figure 7 for the three regions, from PTV (a) and DNS (b). We confirm the predominant alignment of $\boldsymbol{\omega}$ and $\boldsymbol{\lambda_2}$ visible in region A. The probability of this alignment is decreased in region B and region C is characterized by a strong suppression of the preferential ($\boldsymbol{\omega}$,$\boldsymbol{\lambda_2}$) alignment.

Figure 8 shows PDF's of the eigenvalues of the rate of strain tensor, as obtained from PTV (a) and DNS (b). The positively skewed PDF of the intermediate eigenvalue, Λ_2, comprises another genuine property of turbulence (Tsinober, 2001). We see that this property is preserved throughout the three regions. Also the ratio Λ_1:Λ_2:-Λ_3=5:1:6 remains roughly constant and is consistent with the ratios previously reported by others (e.g., Lüthi et al., 2005, Tsinober, 2001, and references therein).

CONCLUSIONS

In summary, we analyzed small scale enstrophy and strain dynamics in proximity of a turbulent/non-turbulent interface without strong mean shear by using 3D-PTV and DNS. The experimental results are in good agreement with the simulation, at least on a qualitative level, which is considered as a clear indication for the reliability of both methods. We found that both $\omega_i\omega_j s_{ij}$ and $\nu\omega_i\nabla^2\omega_i$ are responsible for the increase of ω^2 at the interface and substantiate the physical interpretation of the term $\nu\omega_i\nabla^2\omega_i$ as *viscous interaction*, in analogy to $\omega_i\omega_j s_{ij}$, commonly referred to as the *inviscid interaction* of vorticity and strain. Furthermore, we found that the properties of enstrophy production, $\omega_i\omega_j s_{ij}$, are different in such regions. In particular, vorticity is somewhat more aligned with the vortex stretching vector in the intermediate region B, as compared to regions A and C. In addition, region C is characterized by suppression of the preferential ($\boldsymbol{\omega}$,$\boldsymbol{\lambda_2}$) alignment.

ACKNOWLEDGEMENTS

We gratefully acknowledge the support of this work by ETH Grant No. 0-20151-03. The work of N. Nikitin was supported by the Russian Foundation for Basic Research under the grant 05-01-00607.

REFERENCES

Ashurst, W.T., Kerstein, A.R., Kerr, R.A. and Gibson, C.H., 1987, "Alignment of vorticity and scalar gradient with strain rate in simulated Navier-Stokes turbulence," *Phys. Fluids*, **30**, 23432353.

Batchelor, G.K., 2000, "An Introduction to Fluid Dynamics." *Cambridge University Press.*

Bisset, D.K., Hunt, J.C.R. and Rogers, M.M., 2002, "The turbulent/non-turbulent interface," *J. Fluid Mech.*, **451**, 383-410.

Corrsin, S. and Kistler, A.L., 1954 and 1955, "The free-stream boundaries of turbulent flows," *NACA*, TN-3133 and TR-1244, 1033-1064.

Holzner, M., Liberzon, A., Guala, M., Tsinober, A., Kinzelbach, W., 2006, "Generalized detection of a turbulent front generated by an oscillating grid," *Exp. in Fluids*, **41**(5), 711 - 719.

Holzner, M., Liberzon, A., Nikitin, N., Kinzelbach, W., Tsinober, A., 2007, "Small scale aspects of flows in proximity of the turbulent/non-turbulent interface," accepted for publication in *Phys. Fluids.*

Hoyer, K., Holzner, M., Lüthi, B., Guala, M., Liberzon, A. and Kinzelbach, W., 2005, "3D scanning particle tracking velocimetry," *Exp. Fluids*, **39**(5), 923 - 934.

Lüthi, B., Tsinober, A., Kinzelbach, W., 2005, "Lagrangian Measurement of Vorticity Dynamics in Turbulent Flow," *J. Fluid Mech.*, **528**, 87-118.

Mathew, J., Basu, A.J., 2002, "Some characteristics of entrainment at a cylindrical turbulence boundary," *Phys. of Fluids*, **14**(7), 2065-2072.

Nikitin, N., 1994, "A spectral finite-difference method of calculating turbulent flows of an incompressible fluid in pipes and channels," *Comp. Maths Math. Phys.*, **34**(6), 785798.

Nikitin, N., 1996, "Statistical characteristics of wall turbulence," *Fluid Dynamics*, **31**, 361-370.

Siggia, E.D., 1981, "Numerical study of small-scale intermittency in three-dimensional turbulence," *J. Fluid Mech.*, **107**, 375406.

Townsend, A.A., 1976, "The structure of turbulent shear flow," *Cambridge Univ. Press, London.*

Tsinober, A., 2001, "An informal introduction to turbulence," *Kluwer Academic Publishers.*

Westerweel, J., Fukushima, C., Pedersen, J.M., & Hunt J., 2005, "Mechanics of the Turbulent-Nonturbulent Interface of a Jet," *Phys. Rev. Lett.* **95**, 174501.